


Origin of Low- and High-Energy Monopole Collectivity in ^{132}Sn

Nikolay N. Arsenyev ^{1,*}  and Alexey P. Severyukhin ^{1,2,*} 

¹ Bogoliubov Laboratory of Theoretical Physics, Joint Institute for Nuclear Research, 141980 Dubna, Moscow Region, Russia

² Engineering Physics Institute, Dubna State University, 141982 Dubna, Moscow Region, Russia

* Correspondence: arsenev@theor.jinr.ru (N.N.A.); sever@theor.jinr.ru (A.P.S.)

† These authors contributed equally to this work.

Abstract: Beginning with the Skyrme interaction, we study the properties of the isoscalar giant monopole resonances (ISGMR) of ^{132}Sn . Using the finite-rank separable approximation for the particle-hole interaction, the coupling between one- and two-phonon terms in the wave functions of excited states is taken into account in very large configurational spaces. The inclusion of the phonon–phonon coupling (PPC) results in the formation of a low-energy 0^+ state. The PPC inclusion leads to a fragmentation of the ISGMR strength to lower energy states and also to a higher energy tail. Using the same set of parameters, we describe the available experimental data for the ISGMR characteristics of $^{118,120,122,124}\text{Sn}$ and give a prediction for $^{126,128,130,132}\text{Sn}$.

Keywords: collective levels; giant resonances; nuclear density functional theory

PACS: 21.10.Re; 21.60.Jz; 24.30.Cz



Citation: Arsenyev, N.N.; Severyukhin, A.P. Origin of Low- and High-Energy Monopole Collectivity in ^{132}Sn . *Universe* **2021**, *7*, 145. <https://doi.org/10.3390/universe7050145>

Academic Editor: David Blaschke, Konstantin Maslov, Elena Litvinova and Evgeni Kolomeitsev

Received: 10 March 2021
Accepted: 7 May 2021
Published: 13 May 2021

Publisher's Note: MDPI stays neutral with regard to jurisdictional claims in published maps and institutional affiliations.



Copyright: © 2021 by the authors. Licensee MDPI, Basel, Switzerland. This article is an open access article distributed under the terms and conditions of the Creative Commons Attribution (CC BY) license (<https://creativecommons.org/licenses/by/4.0/>).

1. Introduction

The study of nuclear giant resonances has long been a subject of extensive theoretical and experimental research. The multipole response of nuclei far from the β -stability line and the possible occurrence of exotic modes of excitation represent a growing field of research. In particular, at present, the study of monopole excitations in neutron-rich nuclei is an important problem, not only from the nuclear structure point of view [1], but also because of the special role they play in many astrophysical processes, such as prompt supernova explosions [2,3] and the interiors of neutron stars [4,5]. The experimental source of information regarding incompressibility is isoscalar giant monopole resonances (ISGMR) excited by the inelastic scattering of various projectiles at small angles (see, e.g., [6–11]). A complete list of references on that subject is given in [12]. On the theoretical side, the standard tools for ISGMR studies are random phase approximation (RPA) and quasiparticle RPA (QRPA) in the case of open-shell nuclei in which the self-consistent mean-field is derived from effective nucleon–nucleon interactions that are taken as nonrelativistic two-body Skyrme [13–23] or Gogny [15,24–26] forces. They are also derived from relativistic Lagrangians, e.g., [17,22,27–29]. The effects of the quasiparticle–phonon interaction are important for the damping properties of the ISGMR [25,30–34]. Thanks to experimental advancements, especially at rare isotope beam facilities, the investigation of GMR energies of neutron-rich nuclei along long isotope chains has recently become possible, facilitating more accurate and extensive analyses of the isospin dependence of the incompressibility of infinite nuclear matter. The results of one of the most recent analyses of the experimental data are published in [35]. It was found that the experimental GMR energies are significantly lower than those predicted by recent nonrelativistic and relativistic calculations. The low-energy monopole collectivity in doubly magic nuclei remains an open question. The collective character of the lowest two-phonon (LTP) 0^+ state is mainly the result of coupling to the ISGMR. It is important to note that the pair-transfer mode (see, e.g., [36–39]) is outside of the scope of the present study.

The properties of the LTP 0^+ state are intimately related to the deviation from the harmonic picture for the multiphonon excitations based on the phonon concept [40,41]. In ^{208}Pb , the octupole vibration is lowest in terms of energy and the LTP 0^+ state was first observed as the lowest-spin member of the $[3_1^- \otimes 3_1^-]$ multiplet [42]. As proposed in [34,43], the extension of the variational space from standard QRPA to two-phonon configurations results in the formation of the low-energy 0^+ states. The self-consistent RPA calculation gives the first 0^+ state above 11 MeV in the case of ^{132}Sn [21]. It would be helpful to study the properties of the LTP 0^+ state. The lowest excited state is the 2^+ state at 4.04 MeV [44]. The crucial contribution to the wave function of the 2_1^+ state comes from the one-phonon configuration [45]. This means that the LTP 0^+ energy is less than the double energy of the 2_1^+ RPA state.

The main aim of the present paper is to describe the change in the monopole strength function profile caused by the 2p-2h fragmentation and to analyze its impact on the characteristics of the ISGMR in even–even Sn isotopes close to the $N = 82$ closed shell.

2. The FRSA Model

The tool we employed was the QRPA with Skyrme interaction in the finite rank separable approximation (FRSA) [46,47]. It is worth mentioning that the so-called FRSA has been successfully used to study the electromagnetic transitions between excited states [48,49] and the ISGMR strength distribution within and beyond the QRPA [34,43]. The eigenvalues of the QRPA equations are found numerically as the roots of a relatively simple secular equation, which allows one to perform the calculation in large configurational space [46]. In particular, the cut-off of the discretized continuous part of the single-particle (SP) spectra is at the energy of 100 MeV. Because of this large configurational space, we do not need effective charges. In the present work, calculations were performed with three parameter sets of the Skyrme force, namely, SGII [50], SkM* [51], and Sly4 [52], which have an incompressibility (K_∞) of 215, 217, and 230 MeV, respectively. The pairing correlations were generated by a zero-range surface force and the pairing strength, V_0 , was taken as -750 , -810 , and -870 MeV fm^3 for SkM*, SGII, and Sly4, respectively. To limit the pairing single-particle space, we used the smooth cut-off at 10 MeV above the Fermi energies [47,53]. Taking into account the basic ideas of the quasiparticle–phonon model (QPM) [54], the Hamiltonian was then diagonalized in a space spanned by states composed of one- and two-QRPA phonons [45],

$$\Psi_\nu(JM) = \left(\sum_i R_i(J\nu) Q_{JM_i}^+ + \sum_{\lambda_1 \lambda_2 i_1 i_2} P_{\lambda_2 i_2}^{\lambda_1 i_1}(J\nu) \left[Q_{\lambda_1 \mu_1 i_1}^+ Q_{\lambda_2 \mu_2 i_2}^+ \right]_{\lambda\mu} \right) |0\rangle, \quad (1)$$

where λ denotes the total angular momentum and μ is its z-projection in the laboratory system. The ground state is the QRPA phonon vacuum $|0\rangle$ and the wave functions of excited states (1) are composed of a mixture of 1p-1h and 2p-2h configurations that form the one-phonon $Q_{\lambda_1 \mu_1 i_1}^+ |0\rangle$ and two-phonon components $\left[Q_{\lambda_1 \mu_1 i_1}^+ Q_{\lambda_2 \mu_2 i_2}^+ \right]_{\lambda\mu} |0\rangle$. Using the variational principle, the amplitudes $R_i(\lambda\nu)$ and $P_{\lambda_2 i_2}^{\lambda_1 i_1}(\lambda\nu)$ are determined from a set of linear equations, which have the same form as the QPM equations [55], but the SP spectrum and the parameters of the residual interaction are derived from the chosen Skyrme forces without any further adjustments [45]. To construct the wave functions (1) of the 0^+ states, in the present study, we take all the two-phonon configurations below 30 MeV that are built from the phonons with different multiplicities $\lambda^\pi = 0^+, 1^-, 2^+, 3^-, 4^+$ and 5^- coupled to 0^+ into account. The rank of the set of linear equations is equal to the number of the one- and two-phonon configurations included in the wave function (1). This means that the two-phonon configurational space is now enlarged by the phonon compositions $[\lambda_1^{\pi_1} \otimes \lambda_2^{\pi_2}]_{QRPA}$, i.e., $[0^+ \otimes 0^+]_{QRPA}$, $[1^- \otimes 1^-]_{QRPA}$, $[2^+ \otimes 2^+]_{QRPA}$, $[3^- \otimes 3^-]_{QRPA}$, $[4^+ \otimes 4^+]_{QRPA}$, and $[5^- \otimes 5^-]_{QRPA}$. As an example, for ^{124}Sn , in the case of the set Sly4, the phonon–phonon coupling (PPC) calculation takes into account 64 monopole phonons,

69 dipole phonons, 216 quadrupole phonons, 195 octupole phonons, 236 hexadecapole phonons, and 199 pentapole phonons when all the one- and two-phonon configurations below 30 MeV are included. It is worth mentioning that there are many noncollective two-phonon states in the energy region around the main peak of the giant resonance, paying attention to the violation of the Pauli principle. As proposed in [34], the PPC can be simulated by means of the random distribution of the coupling matrix elements, and the energies of the two-phonon states are generated from the distributions of the Gaussian orthogonal ensemble. The satisfactory description of the results of the microscopic calculations demonstrates a minor role of the Pauli principle corrections for the giant-resonance region.

It is interesting to study the energies, reduced transition probabilities, and the structure of the lowest 2^+ , 3^- , 4^+ and 5^- RPA states, which are the important ingredients of the FRSA model for understanding the nature of the two-phonon 0^+ states of ^{132}Sn . First, the properties of the low-lying states were studied within the one-phonon approximation. The RPA calculations with the sets SLy4, SGII, and SkM* give similar tendencies for the structure. The results of the RPA calculation for the energies, the $B(E\lambda)$ values, and the main two-quasiparticle configurations are given in Table 1. Note that the energies and the reduced transition probabilities calculated within the FRSA are very close to those calculated in the RPA with the original p-h Skyrme interactions [56]. The overestimates regarding energies indicate that there is room for the PPC effects, see Table 2. One can see that the inclusion of the two-phonon terms results in a decrease in the energies and a reduction in the $B(E\lambda)$ values. The crucial contribution in the wave function comes from the RPA one-phonon configuration. The results are in reasonable agreement with the experimental data [44,57,58]. It is worth mentioning that the first discussion of the PPC effect on the 2_1^+ and 3_1^- properties calculated with Skyrme forces was published in [45].

The excitation operator of the ISGMR can be defined as

$$\hat{M}_{\lambda=0} = \sum_{i=1}^A r_i^2. \quad (2)$$

Using the excitation energies E_ν and the transition probabilities $|\langle 0_\nu^+ | \hat{M}_{\lambda=0} | 0_{g.s.}^+ \rangle|^2$, the isoscalar monopole strength distribution is averaged out by a Lorentzian distribution with a width of 1.0 MeV as follows:

$$S(\omega) = \sum_\nu |\langle 0_\nu^+ | \hat{M}_{\lambda=0} | 0_{g.s.}^+ \rangle|^2 \frac{1}{2\pi} \frac{\Delta}{(\omega - E_\nu)^2 + \Delta^2/4}. \quad (3)$$

The excitation energy of the ISGMR is often calculated using the energy-weighted moments of the transition strength:

$$m_k = \sum_\nu (E_\nu)^k |\langle 0_\nu^+ | \hat{M}_{\lambda=0} | 0_{g.s.}^+ \rangle|^2. \quad (4)$$

Tentative estimates for the position of the resonance centroid E_c are defined by $E_c = m_1/m_0$, which is close to the peak energy of the ISGMR, if it is a single peak.

Table 1. Energies, transition probabilities, and structures of the RPA low-lying states: 2_1^+ , 3_1^- , 4_1^+ , and 5_1^- of ^{132}Sn using the Skyrme forces SLy4, SGII, and SkM*. The $B(E\lambda; \lambda_1^\pi \rightarrow 0_{gs}^+)$ values are given in Weisskopf units. The two-quasiparticle configuration contributions greater than 10% are given.

	λ_1^π	Energy (MeV)	$B(E\lambda; \lambda_1^\pi \rightarrow 0_{gs}^+)$ (W.u.)	Structure
SLy4	$[2_1^+]_{RPA}$	4.5	6.9	61% $\{2f_{7/2} 1h_{11/2}\}_\nu$ 33% $\{2d_{5/2} 1g_{9/2}\}_\pi$
	$[3_1^-]_{RPA}$	5.5	28.0	12% $\{1i_{13/2} 1h_{11/2}\}_\nu$ 12% $\{2f_{7/2} 3s_{1/2}\}_\nu$ 16% $\{1h_{11/2} 1g_{9/2}\}_\pi$ 11% $\{1g_{7/2} 2p_{1/2}\}_\pi$
	$[4_1^+]_{RPA}$	5.1	11.3	66% $\{2f_{7/2} 1h_{11/2}\}_\nu$ 19% $\{2d_{5/2} 1g_{9/2}\}_\pi$
	$[5_1^-]_{RPA}$	6.9	8.5	85% $\{2f_{7/2} 2d_{3/2}\}_\nu$
	SkM*	$[2_1^+]_{RPA}$	4.3	6.0
$[3_1^-]_{RPA}$		4.6	22.0	22% $\{2f_{7/2} 3s_{1/2}\}_\nu$ 14% $\{2f_{7/2} 2d_{3/2}\}_\nu$ 11% $\{1i_{13/2} 1h_{11/2}\}_\nu$ 10% $\{1h_{11/2} 1g_{9/2}\}_\pi$
$[4_1^+]_{RPA}$		4.8	9.5	75% $\{2f_{7/2} 1h_{11/2}\}_\nu$ 13% $\{2d_{5/2} 1g_{9/2}\}_\pi$
$[5_1^-]_{RPA}$		5.5	4.9	92% $\{2f_{7/2} 2d_{3/2}\}_\nu$
SGII		$[2_1^+]_{RPA}$	4.3	7.0
	$[3_1^-]_{RPA}$	4.5	27.5	16% $\{2f_{7/2} 3s_{1/2}\}_\nu$ 12% $\{1i_{13/2} 1h_{11/2}\}_\nu$ 11% $\{1h_{11/2} 1g_{9/2}\}_\pi$ 11% $\{1g_{7/2} 2p_{1/2}\}_\pi$
	$[4_1^+]_{RPA}$	4.8	13.3	49% $\{2f_{7/2} 1h_{11/2}\}_\nu$ 24% $\{1g_{7/2} 1g_{9/2}\}_\pi$ 13% $\{2d_{5/2} 1g_{9/2}\}_\pi$
	$[5_1^-]_{RPA}$	6.2	10.6	75% $\{2f_{7/2} 2d_{3/2}\}_\nu$

Table 2. Energies and transition probabilities for the low-lying states 2_1^+ , 3_1^- , 4_1^+ , and 5_1^- of ^{132}Sn using the Skyrme forces SLy4, SGII, and SkM*. The PPC effects are taken into account. The experimental data are taken from [44,57,58]. The $B(E\lambda; \lambda_1^\pi \rightarrow 0_{gs}^+)$ values are given in Weisskopf units.

λ_1^π	Energy (MeV)				$B(E\lambda; \lambda_1^\pi \rightarrow 0_{gs}^+)$ (W.u.)			
	Expt.	Theory			Expt.	Theory		
		SLy4	SkM*	SGII		SLy4	SkM*	SGII
2_1^+	4.04	4.4	4.0	3.8	5.5 ± 1.5 4.4 ± 1.0	6.8	5.6	6.3
3_1^-	4.35	5.2	4.2	3.8	> 7.1	26.2	20.1	24.1
4_1^+	4.42	5.0	4.6	4.4	7.7 ± 0.4	11.2	9.0	12.3
5_1^-	4.94	6.9	5.5	6.0	–	8.5	4.8	9.7

3. Results and Discussion

We begin our discussion of the PPC effects in the case of the even- A $^{118-124}\text{Sn}$ isotopes because the strength distributions for these nuclei have been well studied experimentally [10]. Figure 1 shows the calculated ISGMR strength distributions of $^{118-122}\text{Sn}$ together with the experimental data taken from [10]. The strengths were computed with the force SLy4. In all the three nuclei, the QRPA strength distributions are concentrated in a single peak around 17 MeV, which exhausts the energy-weighted sum rule (EWSR), $2\hbar^2 A \langle r^2 \rangle / m$ [12]. This conclusion remains valid for the sets SGII and SkM*.

A two-phonon triplet of levels was found experimentally [59]. The low-lying levels of ^{124}Sn were explored using the $(n, n'\gamma)$ reaction to identify the LTP 0^+ state. The first 0^+ state at 2.192 MeV is the 0^+ member of the 2^+ two-phonon triplet. For all the three interactions, one of the main components of the wave function is the configuration $[2_1^+ \otimes 2_1^+]_{QRPA}$ (>52%). In the case of the force SLy4, the PPC calculations give a LTP 0^+ state that is significantly higher ($E_x = 4.6$ MeV) than the experimental two-phonon candidate. The set SGII gives the LTP 0^+ state at an energy of 3.4 MeV. The set SkM* gives a 0^+ energy of 2.5 MeV, which is in good agreement with the data.

Let us examine the ISGMR strength distribution of ^{124}Sn (see Figure 2). In the case of the set SLy4 ($K_\infty = 230$ MeV), the ISGMR peak at $E_x = 16.7$ MeV is given as 62% of the EWSR value. For comparison, the set SkM* ($K_\infty = 217$ MeV) gives a stronger splitting of the resonance, as can be seen from Figure 2c. The main peak appears at 16.3 MeV, which exhausts about 36% of the EWSR value. At the same time, the force SGII ($K_\infty = 215$ MeV) gives the ISGMR peak at $E_x = 16.7$ MeV, which exhausts 37% of the EWSR value. In general, we can say that the calculated strength distributions are very similar. The PPC effects on the strength distribution is illustrated in Figures 1 and 2. One can see that both the theoretical and experimental [10] results show the fragmentation and splitting of the ISGMR strength. The results that take into account the PPC (solid curve) indicate a noticeable redistribution of ISGMR strength as compared with those without the PPC effects (dashed curve). There is the low-energy part, the main peak, and the high-energy tail. The QRPA analysis shows that about 95% of the strength of ^{124}Sn , i.e., 95% of the non energy-weighted sum rules (NEWSR), is located at $E_x = 10.5\text{--}20.5$ MeV and the inclusion of the PPC effects leads to a decrease to 68% in the case of the set SLy4. At the same time, the PPC effects shift about 15% (12%) of the strength from the ISGMR region to the high (lower) energy region. Moreover, the PPC effect is a 600 keV downward shift in the ISGMR centroid energy ($E_c = 16.6$ MeV in the one-phonon approximation). As a consequence, about 74% of the total EWSR remains in the ISGMR region. The experimental EWSR value and centroid are $77 \pm 5\%$ and 15.3 ± 0.1 MeV, respectively. Actually the PPC result for the ISGMR centroid energy ($E_c = 15.9$ MeV) and the EWSR value (about 69%) obtained with the force SkM* describes the experimental values [10]. For other choices of Skyrme forces, the strength distribution of the ISGMR obtained within the PPC is also close to the experimental distribution (see Figure 2). In fact, the inclusion of the coupling with the complex configurations plays a key role in explaining the peculiarities of the ISGMR strength distributions in all the considered nuclei (Figures 1 and 2). We found similar tendencies for the neutron-rich Sn isotopes. Considering the feasibility of the experimental study of the ISGMR of $^{126,128,130}\text{Sn}$, we predicted the ISGMR strength distributions. One can see from Figure 3 that the PPC induces a noticeable redistribution of the ISGMR strength as compared with the QRPA results. It is worth mentioning that the role of the quasiparticle–phonon interaction in the case of $^{118,120,122,124}\text{Sn}$ is explained in [33].

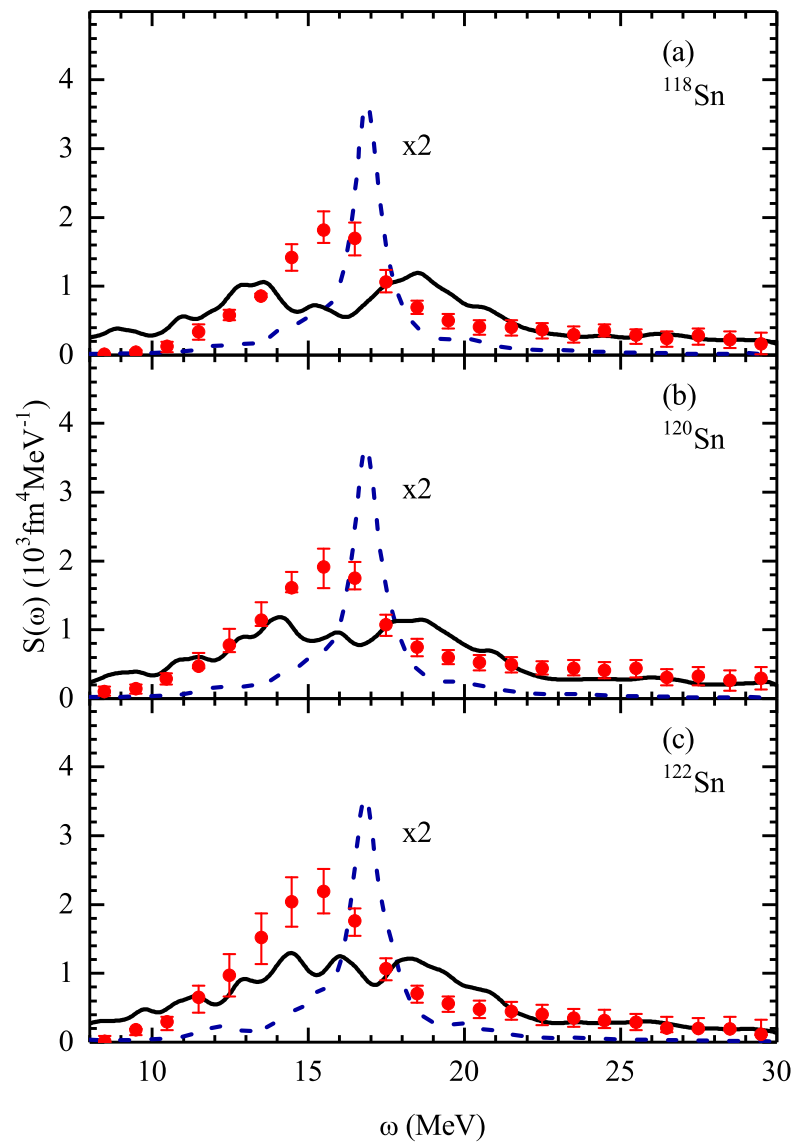


Figure 1. The calculated ISGMR strength distributions for ^{118}Sn (panel (a)), ^{120}Sn (panel (b)), and ^{122}Sn (panel (c)) are compared with the experimental data from [10]. The QRPA results (dashed curves) are scaled down by a factor of 2 for a better display. The solid curves correspond to the results obtained by means of the coupling between the one- and two-phonon configuration. The distributions were calculated with the Skyrme force SLy4. The smoothing parameter 1 MeV was used for the strength distribution described by the Lorentzian function.

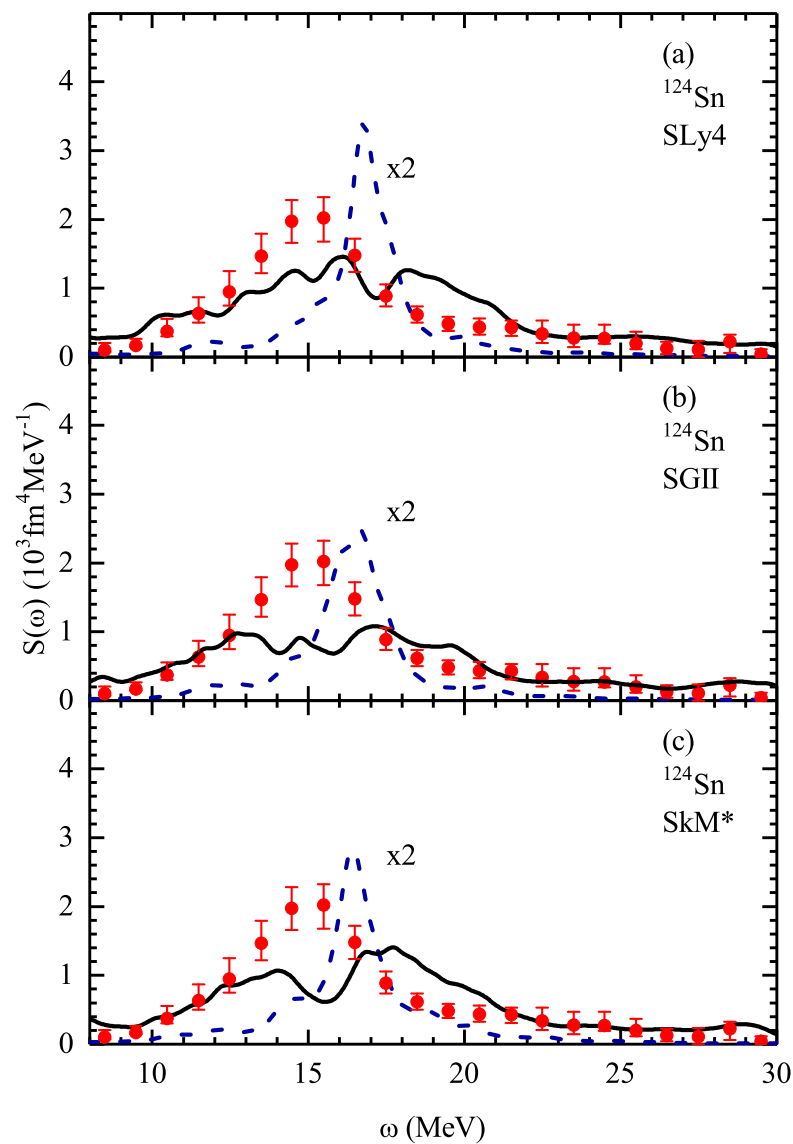


Figure 2. The calculated ISGMR strength distributions in ^{124}Sn are compared with the experimental data from [10] using the Skyrme forces SLy4 (panel (a)), SGII (panel (b)), and SkM* (panel (c)). The QRPA results (dashed curves) are scaled down by a factor of 2 for a better display. The solid curves correspond to the results obtained by means of the coupling between the one- and two-phonon configuration. The smoothing parameter 1 MeV was used for the strength distribution described by the Lorentzian function.

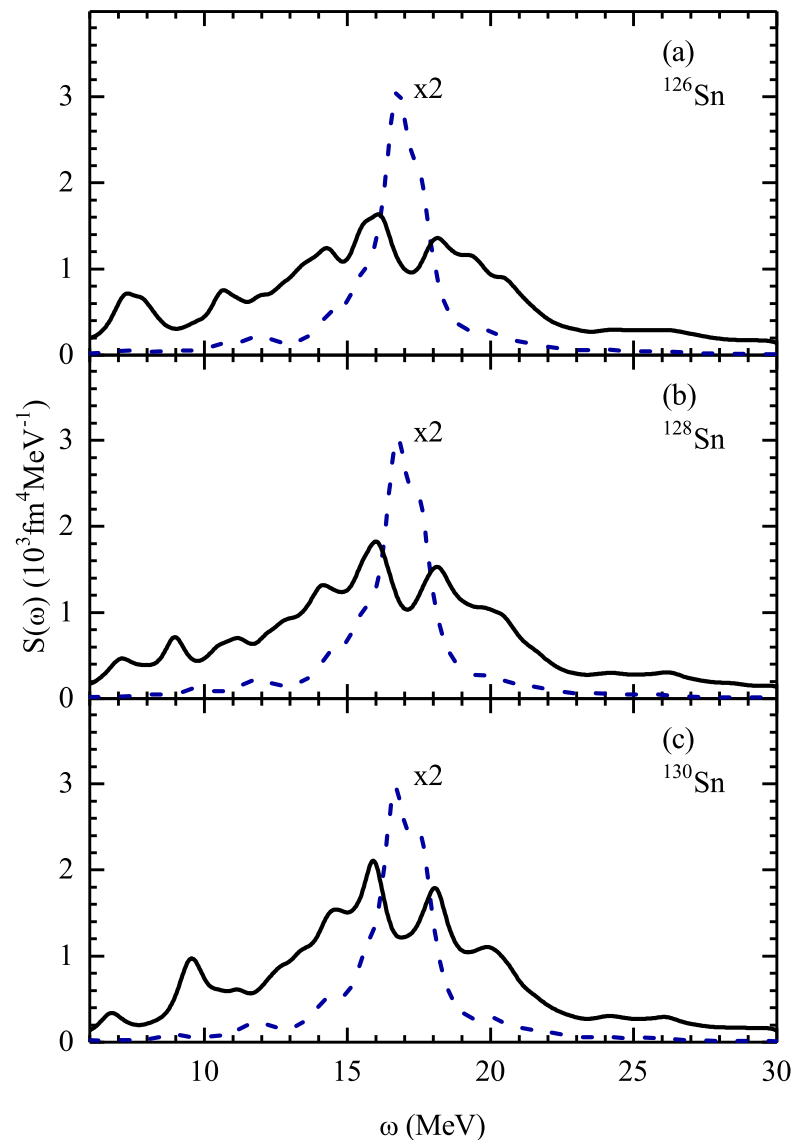


Figure 3. As in Figure 1, for ^{126}Sn (panel (a)), ^{128}Sn (panel (b)), and ^{130}Sn (panel (c)), the distributions were calculated with the Skyrme force SLy4.

Let us now discuss the case of ^{132}Sn . The calculated ISGMR strength distributions are displayed in Figure 4. The results of the RPA calculation are shown in Figure 4a. There are two main peaks at 16.6 MeV and 17.5 MeV. The ISGMR strength in the energy range 10.5–20.5 MeV exhausts 97% of the NEWSR. We found the energy centroid of $E_c = 16.7$ MeV in the energy range. Figure 4b demonstrates the PPC impact on the strength distribution. We found the decrease in the fraction of NEWSR to be 74% and the downward shift in the energy centroid at 0.5 MeV. The PPC induces fragmentation in the high-energy peaks (about 12% of the fraction of NEWSR). The 12% contribution of NEWSR is also moved downwards. Figure 5 shows that our calculations with the force SkM* do not change the above conclusions. In this case, the PPC effects shift about 11% (12%) of the strength from the ISGMR region to the high (lower) energy region. Moreover, the PPC effect is a 700 keV downward shift in the ISGMR centroid energy.

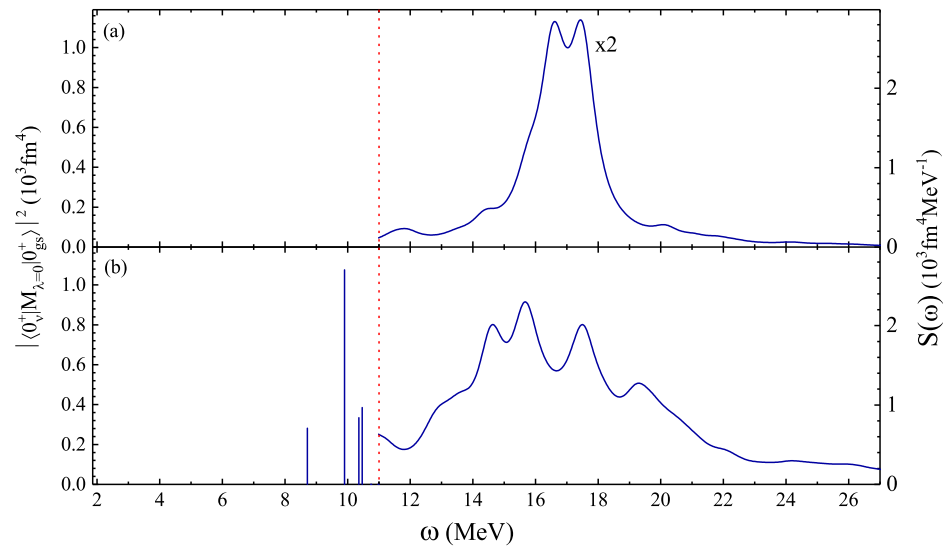


Figure 4. The phonon–phonon coupling effect on the ISGMR of ^{132}Sn . The RPA results (top panel (a)) are scaled down by a factor of 2 for a better display. The results obtained with inclusion of the PPC effects are given in the bottom panel (b). The distributions were calculated with the Skyrme force SLy4. The unit of transition probabilities (the strength function) refers to the vertical axis on the left-hand (right-hand) side. The smoothing parameter 1 MeV was used for the strength distribution described by the Lorentzian function.

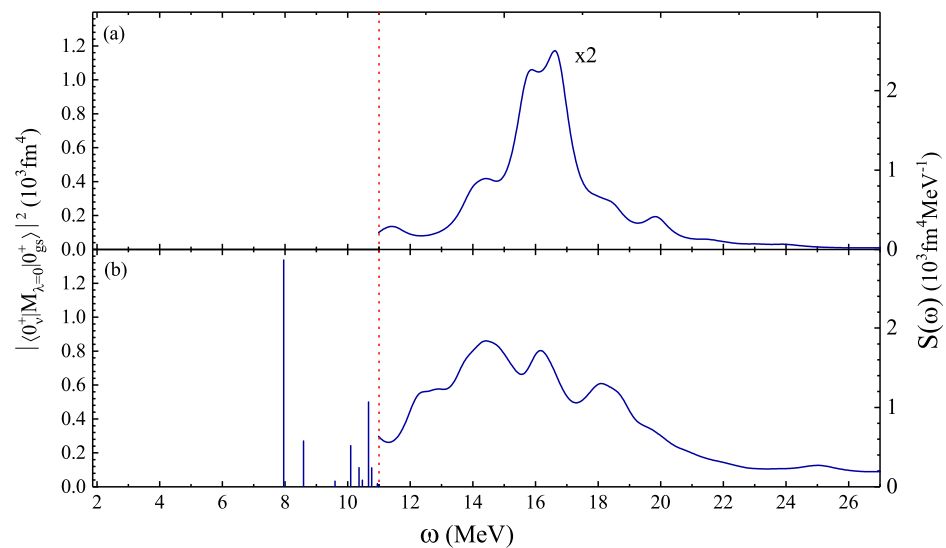


Figure 5. The Skyrme force SkM* is as described in Figure 4.

We found the sequence of collective 0^+ states with common features, located below $E_x < 10.5$ MeV, as shown in Figure 4a. To understand the origin of the low-energy monopole collectivity, let us analyze the wave-function structure of these states. The first one-phonon RPA state appears above 11.5 MeV [21]. The extension of the variational space from the standard RPA to include the two-phonon configurations has a strong effect on the low-energy 0^+ spectrum of ^{132}Sn . As can be seen in the left-hand side of Figure 4, the inclusion of the two-phonon terms results in the formation the low-lying 0^+ states. The 0^+ energies, the largest contributions to the wave function normalization, and the NEWSR fraction are given in column B in Table 3. One can see that the wave functions of the excited $0^+_{1,2,3}$ states of ^{132}Sn are dominated by two-phonon configurations (>90%). The $[2^+ \otimes 2^+]_{RPA}$ configuration is the crucial component of the wave function of the LTP

0^+ state since the 2_1^+ RPA state is the lowest collective excitation, which leads to the minimal two-phonon energy and the maximal matrix elements coupling one- and two-phonon configurations. The energy for the LTP 0^+ state is slightly less than the double energy of the 2_1^+ RPA state (see Table 1). As a result, the inclusion of the 2p-2h neutron configuration $\{2f_7/2 2f_7/2 1h_{11/2} 1h_{11/2}\}_\nu$ plays a considerable role in the calculations of the first excited 0^+ state of ^{132}Sn . We found that the two-phonon configurations $[3_1^- \otimes 3_1^-]_{RPA}$ and $[4_1^+ \otimes 4_1^+]_{RPA}$ are split between the excited 0_2^+ and 0_3^+ states. On the other hand, the wave function of the $0_{2,3}^+$ states particularly mix 2.1% of the $[0_6^+]_{RPA}$ and 2.9% of the $[0_8^+]_{RPA}$ configurations into the 0_2^+ state; and 1.0% of the $[0_6^+]_{RPA}$ and 1.2% of the $[0_8^+]_{RPA}$ configurations into the 0_3^+ state. This small change in the structure has a large effect on the $|\langle 0_{2,3}^+ | \hat{M}_{\lambda=0} | 0_{g.s.}^+ \rangle|^2$ values. To check the structure for the low-lying 0^+ states, the PPC calculations were performed in the space of all the one- and two-phonon configurations with energies up to 25 MeV (column A in Table 3) and 30 MeV (column B in Table 3), respectively. The obtained results demonstrate the expected unimportance of the high-energy configurations. On the other hand, the structure of LTP 0^+ states of ^{132}Sn is dependent on the choice of Skyrme parametrizations (see column B in Table 3). It is well known that the single-particle spectra around the Fermi level are key for microscopic analyses. In the case of the force SkM*, we found that the main components of the 0_1^+ wave function are the $[2_1^+ \otimes 2_1^+]_{RPA}$ and $[3_1^- \otimes 3_1^-]_{RPA}$ configurations. In addition, the structure of the first 0^+ state comes from the 2.5% mix of the $[0_6^+]_{RPA}$ and 2.7% of the $[0_8^+]_{RPA}$ configurations. These configurations give the crucial contribution in the $|\langle 0_1^+ | \hat{M}_{\lambda=0} | 0_{g.s.}^+ \rangle|^2$ value, as shown in Figure 5a. Clearly, further theoretical and experimental studies are required to provide additional insight into the low-energy structure of excited 0^+ states.

Table 3. Energies, dominant RPA components of phonon structures, and NEWSR fraction of the LTP 0^+ states of ^{132}Sn using the Skyrme forces SLy4, SGII, and SkM*. Columns (A) and (B) give the values calculated in the space of all the one- and two-phonon configurations with energies up to 25 MeV and 30 MeV, respectively.

	λ_i^π	Energy (MeV)		Structure		NEWSR Fraction	
		A	B	A	B	A	B
SLy4	0_1^+	8.8	8.7	96% $[2_1^+ \otimes 2_1^+]_{RPA}$	93% $[2_1^+ \otimes 2_1^+]_{RPA}$	1.1%	1.6%
	0_2^+	10.0	9.9	61% $[4_1^+ \otimes 4_1^+]_{RPA}$ +27% $[3_1^- \otimes 3_1^-]_{RPA}$	49% $[4_1^+ \otimes 4_1^+]_{RPA}$ +34% $[3_1^- \otimes 3_1^-]_{RPA}$	5.0%	6.0%
	0_3^+	10.4	10.4	55% $[3_1^- \otimes 3_1^-]_{RPA}$ +37% $[4_1^+ \otimes 4_1^+]_{RPA}$	47% $[4_1^+ \otimes 4_1^+]_{RPA}$ +43% $[3_1^- \otimes 3_1^-]_{RPA}$	3.2%	1.9%
SkM*	0_1^+	8.1	8.0	46% $[2_1^+ \otimes 2_1^+]_{RPA}$ +39% $[3_1^- \otimes 3_1^-]_{RPA}$	42% $[3_1^- \otimes 3_1^-]_{RPA}$ +38% $[2_1^+ \otimes 2_1^+]_{RPA}$	6.5%	7.8%
	0_2^+	8.6	8.6	52% $[2_1^+ \otimes 2_1^+]_{RPA}$ +43% $[3_1^- \otimes 3_1^-]_{RPA}$	59% $[2_1^+ \otimes 2_1^+]_{RPA}$ +36% $[3_1^- \otimes 3_1^-]_{RPA}$	1.9%	1.6%
	0_3^+	9.6	9.6	94% $[4_1^+ \otimes 4_1^+]_{RPA}$	92% $[4_1^+ \otimes 4_1^+]_{RPA}$	0.2%	0.2%
SGII	0_1^+	7.7	7.6	62% $[3_1^- \otimes 3_1^-]_{RPA}$ +17% $[2_1^+ \otimes 2_1^+]_{RPA}$	60% $[3_1^- \otimes 3_1^-]_{RPA}$ +16% $[2_1^+ \otimes 2_1^+]_{RPA}$	10.2%	11.4%
	0_2^+	8.5	8.5	80% $[2_1^+ \otimes 2_1^+]_{RPA}$ +19% $[3_1^- \otimes 3_1^-]_{RPA}$	81% $[2_1^+ \otimes 2_1^+]_{RPA}$ +18% $[3_1^- \otimes 3_1^-]_{RPA}$	0.3%	0.3%
	0_3^+	9.5	9.5	93% $[4_1^+ \otimes 4_1^+]_{RPA}$	92% $[4_1^+ \otimes 4_1^+]_{RPA}$	0.2%	0.2%

4. Conclusions

In summary, beginning with the Skyrme mean-field calculations with the Skyrme forces SLy4, SGII, and SkM*, the properties of the spectrum of 0^+ excitations of ^{132}Sn were studied within the FRSA model, including both the PPC effects. The suggested approach enables one to perform the calculations in very large configuration spaces. We applied this

model to understand the ISGMR characteristics of $^{118-132}\text{Sn}$. Our calculation, which takes into account the 2p-2h fragmentation, indicates a monopole strength at a lower energy than the main peak and a high-energy tail above. Our results are in reasonable agreement with the experimental data for $^{118,120,122,124}\text{Sn}$, as reported in [10].

Our initial objective was the prediction of the formation of the collective low-lying 0^+ states in ^{132}Sn , as compared to the standard RPA. The inclusion of the coupling between one- and two-phonon terms in the wave functions of excited states leads to a redistribution of the strength of the ISGMR. A part of the main peak strength is fragmented in the low-energy states and the main peak itself is shifted downwards. The PPC inclusion shifts about 12% of the total monopole strength into the lower energy region ($E_x < 10.5$ MeV) and the higher energy region ($E_x > 20.5$ MeV). The crucial contribution in the wave-function structure of the low-lying 0^+ states ($E_x < 11.6$ MeV) comes from the two-phonon configurations and, in particular, the $[2_1^+ \otimes 2_1^+]_{RPA}$ configuration for the LTP 0^+ state. Moreover, there is a smaller contribution from the one-phonon configurations, which are dominated by the main peaks of the ISGMR. It is shown that the 2p-2h fragmentation leads to an increase in the ISGMR width. Data for the 0^+ spectrum of ^{132}Sn are very scarce. It would be desirable to experimentally establish the LTP 0^+ state identified as the two-phonon state.

Author Contributions: N.N.A. and A.P.S. have contributed equally to this work. Both authors have read and agreed to the published version of the manuscript.

Funding: This work was partly supported by the Heisenberg–Landau (Germany-BLTP JINR) program and the National Research Foundation of South Africa (Grant No. 129603).

Data Availability Statement: Not applicable.

Acknowledgments: We appreciate illuminating discussions with Nguyen Van Giai, N. Pietralla, and H. Sagawa.

Conflicts of Interest: The authors declare no conflict of interest.

References

1. Blaizot, J.P. Nuclear compressibilities. *Phys. Rep.* **1980**, *64*, 171–248. [[CrossRef](#)]
2. Baron, E.; Cooperstein, J.; Kahana, S. Type-II supernovae in $12M_\odot$ and $15M_\odot$ stars: The equation of state and general relativity. *Phys. Rev. Lett.* **1985**, *55*, 126–129. [[CrossRef](#)] [[PubMed](#)]
3. Bethe, H.A. Supernova mechanisms. *Rev. Mod. Phys.* **1990**, *62*, 801–866. [[CrossRef](#)]
4. Glendenning, N.K. Neutron-star masses as a constraint on the nuclear compression modulus. *Phys. Rev. Lett.* **1986**, *57*, 1120–1123. [[CrossRef](#)]
5. Lattimer, J.M.; Prakash, M. Neutron star structure and the equation of state. *Astrophys. J.* **2001**, *550*, 426–442. [[CrossRef](#)]
6. Youngblood, D.H.; Clark, H.L.; Lui, Y.-W. Incompressibility of nuclear matter from the giant monopole resonance. *Phys. Rev. Lett.* **1999**, *82*, 691–694. [[CrossRef](#)]
7. Youngblood, D.H.; Lui, Y.-W.; Clark, H.L.; John, B.; Tokimoto, Y.; Chen, X. Isoscalar $E0 - E3$ strength in ^{116}Sn , ^{144}Sm , ^{154}Sm , and ^{208}Pb . *Phys. Rev. C* **2004**, *70*, 034315. [[CrossRef](#)]
8. Lui, Y.-W.; Youngblood, D.H.; Tokimoto, Y.; Clark, H.L.; John, B. Giant resonances in ^{112}Sn and ^{124}Sn : Isotopic dependence of monopole resonance energies. *Phys. Rev. C* **2004**, *70*, 014307. [[CrossRef](#)]
9. Li, T.; Garg, U.; Liu, Y.; Marks, R.; Nayak, B.K.; Madhusudhana Rao, P.V.; Fujiwara, M.; Hashimoto, H.; Kawase, K.; Nakanishi, K.; et al. Isotopic dependence of the giant monopole resonance in the even- A $^{112-124}\text{Sn}$ isotopes and the asymmetry term in nuclear incompressibility. *Phys. Rev. Lett.* **2007**, *99*, 162503. [[CrossRef](#)] [[PubMed](#)]
10. Li, T.; Garg, U.; Liu, Y.; Marks, R.; Nayak, B.K.; Madhusudhana Rao, P.V.; Fujiwara, M.; Hashimoto, H.; Nakanishi, K.; Okumura, S.; et al. Isoscalar giant resonances in the Sn nuclei and implications for the asymmetry term in the nuclear-matter incompressibility. *Phys. Rev. C* **2010**, *81*, 034309. [[CrossRef](#)]
11. Patel, D.; Garg, U.; Itoh, M.; Akimune, H.; Berg, G.P.A.; Fujiwara, M.; Harakeh, M.N.; Iwamoto, C.; Kawabata, T.; Kawase, K.; et al. Excitation of giant monopole resonance in ^{208}Pb and ^{116}Sn using inelastic deuteron scattering. *Phys. Lett. B* **2014**, *735*, 387–390. [[CrossRef](#)]
12. Garg, U.; Cold, G. The compression-mode giant resonances and nuclear incompressibility. *Prog. Part. Nucl. Phys.* **2018**, *101*, 55–95. [[CrossRef](#)]
13. Giai, N.V.; Sagawa, H. Monopole and dipole compression modes in nuclei. *Nucl. Phys. A* **1981**, *371*, 1–18. [[CrossRef](#)]
14. Agrawal, B.K.; Shlomo, S. Consequences of self-consistency violations in Hartree-Fock random-phase approximation calculations of the nuclear breathing mode energy. *Phys. Rev. C* **2004**, *70*, 014308. [[CrossRef](#)]

15. Colò, G.; Giai, N.V.; Meyer, J.; Bennaceur, K.; Bonche, P. Microscopic determination of the nuclear incompressibility within the nonrelativistic framework. *Phys. Rev. C* **2004**, *70*, 024307. [[CrossRef](#)]
16. Terasaki, J.; Engel, J. Self-consistent description of multipole strength: Systematic calculations. *Phys. Rev. C* **2006**, *74*, 044301. [[CrossRef](#)]
17. Paar, N.; Vretenar, D.; Khan, E.; Colò, G. Exotic modes of excitation in atomic nuclei far from stability. *Rep. Prog. Phys.* **2007**, *70*, 691–793. [[CrossRef](#)]
18. Li, J.; Colò, G.; Meng, J. Microscopic linear response calculations based on the Skyrme functional plus the pairing contribution. *Phys. Rev. C* **2008**, *78*, 064304. [[CrossRef](#)]
19. Khan, E. Role of superfluidity in nuclear incompressibilities. *Phys. Rev. C* **2009**, *80*, 011307(R). [[CrossRef](#)]
20. Cao, L.-G.; Sagawa, H.; Colò, G. Microscopic study of the isoscalar giant monopole resonance in Cd, Sn, and Pb isotopes. *Phys. Rev. C* **2012**, *86*, 054313. [[CrossRef](#)]
21. Yüksel, E.; Khan, E.; Bozkurt, K. The soft giant monopole resonance as a probe of the spin-orbit splitting. *Eur. Phys. J. A* **2013**, *49*, 124. [[CrossRef](#)]
22. Khan, E.; Paar, N.; Vretenar, D.; Cao, L.-G.; Sagawa, H.; Colò, G. Incompressibility of finite fermionic systems: Stable and exotic atomic nuclei. *Phys. Rev. C* **2013**, *87*, 064311. [[CrossRef](#)]
23. Hamamoto, I.; Sagawa, H. Self-consistent Hartree-Fock and RPA Green's function method indicate no pygmy resonance in the monopole response of neutron-rich Ni isotopes. *Phys. Rev. C* **2014**, *90*, 031302(R). [[CrossRef](#)]
24. Péru, S.; Berger, J.F.; Bortignon, P.F. Giant resonances in exotic spherical nuclei within the RPA approach with the Gogny force. *Eur. Phys. J. A* **2005**, *26*, 25–32. [[CrossRef](#)]
25. Gambacurta, D.; Grasso, M.; De Donno, V.; Co', G.; Catara, F. Second random-phase approximation with the Gogny force: First applications. *Phys. Rev. C* **2012**, *86*, 021304(R). [[CrossRef](#)]
26. Péru, S.; Martini, M. Mean field based calculations with the Gogny force: Some theoretical tools to explore the nuclear structure. *Eur. Phys. J. A* **2014**, *50*, 88. [[CrossRef](#)]
27. Piekarewicz, J. Self-consistent description of nuclear compressional modes. *Phys. Rev. C* **2001**, *64*, 024307. [[CrossRef](#)]
28. Ma, Z.-Y.; Wandelt, A.; Giai, N.V.; Vretenar, D.; Ring, P.; Cao, L.-G. Collective multipole excitations in a microscopic relativistic approach. *Nucl. Phys. A* **2002**, *703*, 222–239. [[CrossRef](#)]
29. Vretenar, D.; Nikšić, T.; Ring, P. A microscopic estimate of the nuclear matter compressibility and symmetry energy in relativistic mean-field models. *Phys. Rev. C* **2003**, *68*, 024310. [[CrossRef](#)]
30. Drożdż, S.; Nishizaki, S.; Speth, J.; Wambach, J. The nuclear response within extended RPA theories. *Phys. Rep.* **1990**, *197*, 1–65. [[CrossRef](#)]
31. Kamerdzhev, S.; Speth, J.; Tertychny, G. Microscopic analysis of the breathing mode in ^{40}Ca and ^{58}Ni . *Eur. Phys. J. A* **2000**, *7*, 483–490. [[CrossRef](#)]
32. Litvinova, E.; Ring, P.; Tselyaev, V. Particle-vibration coupling within covariant density functional theory. *Phys. Rev. C* **2007**, *75*, 064308. [[CrossRef](#)]
33. Tselyaev, V.; Speth, J.; Krewald, S.; Litvinova, E.; Kamerdzhev, S.; Lyutorovich, N.; Avdeenkov, A.; Grümmer, F. Description of the giant monopole resonance in the even- A $^{112-124}\text{Sn}$ isotopes within a microscopic model including quasiparticle-phonon coupling. *Phys. Rev. C* **2009**, *79*, 034309. [[CrossRef](#)]
34. Severyukhin, A.P.; Åberg, S.; Arsenyev, N.N.; Nazmitdinov, R.G. Spreading widths of giant resonances in spherical nuclei: damped transient response. *Phys. Rev. C* **2017**, *95*, 061305(R). [[CrossRef](#)]
35. Li, B.-A.; Xie, W.-J. Differential analysis of incompressibility in neutron-rich nuclei. *arXiv* **2021**, arXiv:2102.10683.
36. Blomqvist, J. The $3^- \otimes 3^-$ two-phonon quartet and the proton pairing vibration in ^{208}Pb . *Phys. Lett. B* **1970**, *33*, 541–544. [[CrossRef](#)]
37. Igo, G.J.; Barnes, P.D.; Flynn, E.R. Mixing of two-particle, two-hole states in Pb. *Phys. Rev. Lett.* **1970**, *24*, 470–473. [[CrossRef](#)]
38. Julin, R.; Kantele, J.; Kumpulainen, J.; Luontama, M.; Passoja, A.; Trzaska, W.; Verho, E.; Blomqvist, J. $E0$ study of 0^+ states near 5 MeV in Pb. *Phys. Rev. C* **1987**, *36*, 1129–1131. [[CrossRef](#)]
39. Heusler, A.; Faestermann, T.; Hertenberger, R.; Wirth, H.-F.; von Brentano, P. Identification of the 0^+ proton pairing vibration state in the doubly magic nucleus ^{208}Pb by particle spectroscopy. *Phys. Rev. C* **2015**, *91*, 044325. [[CrossRef](#)]
40. Lanza, E.G.; Andrés, M.V.; Catara, F.; Chomaz, P.; Volpe, C. Role of anharmonicities and nonlinearities in heavy ion collisions a microscopic approach. *Nucl. Phys. A* **1997**, *613*, 445–471. [[CrossRef](#)]
41. Ponomarev, V.Y.; von Neumann-Cosel, P. Fragmentation of the two-octupole phonon multiplet in ^{208}Pb . *Phys. Rev. Lett.* **1999**, *82*, 501–504. [[CrossRef](#)]
42. Yeh, M.; Garrett, P.E.; McGrath, C.A.; Yates, S.W.; Belgya, T. Two-phonon octupole excitation in ^{208}Pb . *Phys. Rev. Lett.* **1996**, *76*, 1208–1211. [[CrossRef](#)]
43. Severyukhin, A.P.; Åberg, S.; Arsenyev, N.N.; Nazmitdinov, R.G.; Pichugin, K.N. Random matrix analysis of the monopole strength distribution in ^{208}Pb . *Phys. At. Nucl.* **2016**, *79*, 835–841. [[CrossRef](#)]
44. Fogelberg, B.; Hellström, M.; Jerrestam, D.; Mach, H.; Blomqvist, J.; Kerek, A.; Norlin, L.O.; Omtvedt, J.P. Detailed spectroscopy of the doubly closed shell nucleus ^{132}Sn : First observation of octupole collectivity. *Phys. Rev. Lett.* **1994**, *73*, 2413–2416. [[CrossRef](#)]
45. Severyukhin, A.P.; Voronov, V.V.; Giai, N.V. Effects of phonon-phonon coupling on low-lying states in neutron-rich Sn isotopes. *Eur. Phys. J. A* **2004**, *22*, 397–403. [[CrossRef](#)]

46. Giai, N.V.; Stoyanov, C.; Voronov, V.V. Finite rank approximation for random phase approximation calculations with Skyrme interactions: An application to Ar isotopes. *Phys. Rev. C* **1998**, *57*, 1204–1209. [[CrossRef](#)]
47. Severyukhin, A.P.; Voronov, V.V.; Giai, N.V. Effects of the particle-particle channel on properties of low-lying vibrational states. *Phys. Rev. C* **2008**, *77*, 024322. [[CrossRef](#)]
48. Severyukhin, A.P.; Arsenyev, N.N.; Pietralla, N. Proton-neutron symmetry in ^{92}Zr , ^{94}Mo with Skyrme interactions in a separable approximation. *Phys. Rev. C* **2012**, *86*, 024311. [[CrossRef](#)]
49. Severyukhin, A.P.; Arsenyev, N.N.; Pietralla, N.; Werner, V. Impact of variational space on $M1$ transitions between first and second quadrupole excitations in $^{132,134,136}\text{Te}$. *Phys. Rev. C* **2014**, *90*, 011306(R). [[CrossRef](#)]
50. Giai, N.V.; Sagawa, H. Spin-isospin and pairing properties of modified Skyrme interactions. *Phys. Lett. B* **1981**, *106*, 379–382. [[CrossRef](#)]
51. Bartel, J.; Quentin, P.; Brack, M.; Guet, C.; Håkansson, H.-B. Towards a better parametrisation of Skyrme-like effective forces: A critical study of the SkM force. *Nucl. Phys. A* **1982**, *386*, 79–100. [[CrossRef](#)]
52. Chabanat, E.; Bonche, P.; Haensel, P.; Meyer, J.; Schaeffer, R. A Skyrme parametrization from subnuclear to neutron star densities part II. Nuclear far form stabilities. *Nucl. Phys. A* **1998**, *635*, 231–256; Erratum in **1998**, *643*, 441. [[CrossRef](#)]
53. Severyukhin, A.P.; Arsenyev, N.N.; Borzov, I.N.; Sushenok, E.O. Multi-neutron emission of Cd isotopes. *Phys. Rev. C* **2017**, *95*, 034314. [[CrossRef](#)]
54. Soloviev, V.G. *Theory of Atomic Nuclei: Quasiparticles and Phonons*; Institute of Physics: Bristol, UK, 1992.
55. Voronov, V.V.; Karadjov, D.; Catara, F.; Severyukhin, A.P. Ground state correlations beyond random phase approximation and collective excitations. *Phys. Part. Nucl.* **2000**, *31*, 452–470.
56. Colò, G.; Bortignon, B.F.; Sarchi, D.; Khoa, D.T.; Khan, E. Giai, N.V. Excited states of neutron-rich nuclei: Mean field theory and beyond. *Nucl. Phys. A* **2003**, *722*, 111c–116c. [[CrossRef](#)]
57. Rosiak, D.; Seidlitz, M.; Reiter, P.; Naïdja, H.; Tsunoda, Y.; Togashi, T.; Nowacki, F.; Otsuka, T.; Colò, G.; Arnsward, K.; et al. Enhanced quadrupole and octupole strength in doubly magic ^{132}Sn . *Phys. Rev. Lett.* **2018**, *121*, 252501. [[CrossRef](#)]
58. Benito, J.; Fraile, L.M.; Korgul, A.; Piersa, M.; Adamska, E.; Andreyev, A.N.; Álvarez-Rodríguez, R.; Barzakh, A.E.; Benzoni, G.; Berry, T.; et al. Detailed spectroscopy of doubly magic ^{132}Sn . *Phys. Rev. C* **2020**, *102*, 014328. [[CrossRef](#)]
59. Bandyopadhyay, D.; Warr, N.; Fransen, C.; Boukharouba, N.; Werner, V.; Yates, S.W.; Weil, J.L.; McEllistrem, M.T. Three-phonon excitations in ^{124}Sn . *Nucl. Phys. A* **2005**, *747*, 206–226. [[CrossRef](#)]